RSC Advances

PAPER

View Article Online
View Journal | View Issue

Cite this: *RSC Adv.*, 2021, **11**, 6259

Bridging-arylene effects on spectroscopic and photophysical properties of arylborane–dipyrrinato zinc(II) complexes†

Koyo Takaki,[a] Eri Sakuda,[a]* Akitaka Ito,[b] Shinnosuke Horiuchi,[a] Yasuhiro Arikawa[a] and Keisuke Umakoshi[a]*

Received 23rd October 2020
Accepted 23rd January 2021

DOI: 10.1039/d0ra09029h

rsc.li/rsc-advances

Novel bis(dipyrrinato)zinc(II) derivatives having 4-[bis(2,4,6-trimethylphenyl)boryl]phenyl (**ZnBph**) or 4-[bis(2,4,6-trimethylphenyl)boryl]-2,3,5,6-tetramethylphenyl groups (**ZnBdu**) at the 5-position of the dipyrrinato ligands were designed and synthesized. In **ZnBph** with the smaller dipyrrinate–arylene and arylene–dimesitylboryl dihedral angles, an intramolecular charge transfer arising from the presence of the vacant p orbital on the boron atom participates in the ππ* excited state in character in contrast to the pure ππ* excited state of **ZnBdu**. The synergistic ππ*/ILCT excited state was weakly fluorescent, and the fluorescence was enhanced upon binding of fluoride to the boron atom.

Introduction

Triarylborane derivatives exhibit a characteristic absorption/fluorescence owing to an intramolecular charge transfer (CT) transition from the π orbital of aryl group to the vacant p orbital on the boron atom (π(aryl)–p(B) CT) and, therefore, various triarylborane derivatives have been reported.[1–11] Triarylboranes are also able to tune the spectroscopic and photophysical properties of a metal complex by being introduced to the periphery of its ligand(s). As a pioneering example reported by Kitamura and coworkers, a $CHCl_3$ solution of $[Pt(Bph\text{-}tpy)Cl]^+$ (Bph-tpy = 4′-{4-[bis(2,4,6-trimethylphenyl)boryl]phenyl}-2,2′:6′,2″-terpyridine) showed intense phosphorescence even at room temperature (emission quantum yield = 0.011) whereas a metal-to-ligand CT (MLCT) excited state of a $[Pt(tpy)Cl]^+$ (tpy = 2,2′:6′,2″-terpyridine) derivative is typically nonemissive in a solution phase.[12] The enhanced emission from $[Pt(Bph\text{-}tpy)Cl]^+$ originates in synergistic CT interactions between MLCT in the Pt(tpy)Cl moiety and π(aryl)–p(B) CT in the triarylborane unit. Interestingly, an analogous complex, $[Pt(Bdu\text{-}tpy)Cl]^+$ (Bdu-tpy = 4′-{4-[bis(2,4,6-trimethylphenyl)boryl]-2,3,5,6-tetramethylphenyl}-2,2′:6′,2″-terpyridine), did not exhibit such room-temperature phosphorescence at all. The difference in the phosphorescence ability between the complexes was explained by a disconnection of the CT systems in $[Pt(Bdu\text{-}tpy)Cl]^+$ due to the perpendicularly-oriented durylene (2,3,5,6-tetramethylphenylene) group. Thus, the triarylborane has become one of the choices to control photophysical/photochemical properties of a metal complex.[13–37] However, the number of the reports focusing on effects of a linker between the triarylborane and metal-complex moieties is still limited.[38–40]

We recently reported synthesis, spectroscopic and photophysical properties of cyclometalated iridium(III)[41] and platinum(II) complexes with an arylborane-appended dipyrrinato ligand(s).[42] These complexes showed intense visible absorption (molar absorption coefficient $\varepsilon \geq 10^4\ M^{-1}\ cm^{-1}$ (M = mol dm^{-3}) at ~490 nm) and visible–near-IR phosphorescence ascribed to the synergistic MLCT/ππ*/π(aryl)–p(B) CT transition. Dipyrrinato metal complexes exhibiting the CT-type excited states are characteristic at this stage since most of the excited states of dipyrrinato metal complexes are ascribed to ππ* transition in the dipyrrinato ligand.[43–52] Especially, two stereoisomers of bis(5-{4-[bis(2,4,6-trimethylphenyl)boryl]phenyl}dipyrrinato)platinum(II), **PtBph**, possessing the square-planar and distorted tetrahedral geometries show different absorption/emission spectra not only in the MLCT/ππ*/π(aryl)–p(B) CT band but also in the ligand-centered (LC) band. Both crystallographic data and theoretical calculations suggest that a dihedral angle between the dipyrrinate and bridging phenylene moieties in the square-planar isomer is larger than that in the distorted tetrahedral one. The results remind us of the earlier Pt-tpy system and importance of further understanding of the ligand itself in an arylborane-appended metal complex.

In order to extract the molecular/electronic effects of the ligand itself in an arylborane–dipyrronato metal complex, we chose dipyrrinato zinc(II) complexes. They exhibit intense visible absorption (absorption maximum wavelength $\lambda_{abs} \approx$ 470–500 nm; $\varepsilon \approx (5.0\text{–}10) \times 10^4\ M^{-1}\ cm^{-1}$) and fluorescence

[a]*Division of Chemistry and Materials Science, Graduate School of Engineering, Nagasaki University, Bunkyo-machi 1-14, Nagasaki 852-8521, Japan. E-mail: sakueri@nagasaki-u.ac.jp; kumks@nagasaki-u.ac.jp*

[b]*Graduate School of Engineering, Kochi University of Technology, Miyanokuchi 185, Tosayamada, Kami, Kochi 782-8502, Japan*

† Electronic supplementary information (ESI) available: ^1H and $^{13}C\{^1H\}$ NMR spectra, crystallographic data of **ZnBdu**, detailed results of theoretical calculations, fluorescence decay profiles and ^1H NMR spectra in the absence and presence of TBAF. CCDC 2035525. For ESI and crystallographic data in CIF or other electronic format see DOI: 10.1039/d0ra09029h

ascribed to pure LC ππ* excited states owing to the inert d^{10} nature of the zinc(II) center.[53–61] Furthermore, the spectroscopic properties of a dipyrrinato zinc(II) complex are dependent on the substituent group at the 5-position of the dipyrrinato ligand. For example, Lindsey and coworkers revealed that bis[5-(2,4,6-trimethylphenyl)dipyrrinato]zinc(II) (**Znmes**) showed much higher fluorescence quantum yield ($\Phi_f = 0.36$) than bis(5-phenyldipyrrinato)zinc(II) (**Znph**, $\Phi_f = 0.01$) by effects of both fluorescent and nonfluorescent pathways.[62] It has also been reported that the fluorescence from **Znmes** is quenched in a polar solvent by a thermal deactivation of the excited state *via* a CT-type state.[58,63,64] These results indicate that structures of aryl groups at 5-position of the dipyrronato ligands and the introduction of intramolecular CT interactions are key points to control the spectroscopic/photophysical properties of a bis(dipyrrinato)zinc(II) complex. The π(aryl)–p(B) CT of an arylborane group is, therefore, one of possible candidates to tune the points. We synthesized novel bis(dipyrrinato)zinc(II) derivatives having 4-(dimesitylboryl)phenyl (**ZnBph**) or (dimesitylboryl) duryl group (mesityl = 2,4,6-trimethylphenyl and duryl = 2,3,5,6-tetramethylphenyl) at 5-position of the dipyrrinato ligands (**ZnBdu**), whose structures are shown in Chart 1. The bridging phenylene and durylene moieties in the complexes gave significant differences especially in the fluorescence and fluoride-binding properties. The characteristic photophysical properties of the former complex (**ZnBph**) can be explained by gained intraligand charge transfer (ILCT) character in the excited state and discussed in terms of the molecular geometries obtained by theoretical calculations.

Experimental section

Chemicals

All the reagents including organic solvents were commercially available and used without further purification. 5-{4-[Bis(2,4,6-trimethylphenyl)boryl]phenyl}dipyrrin was prepared according to the literature methods.[41] 4-[Bis(2,4,6-trimethylphenyl)boryl]-2,3,5,6-tetramethylbenzaldehyde (**2**) was synthesized similarly to the phenyl analogue. All the synthetic reactions and subsequent workup manipulations were carried out under air unless otherwise noted.

Physical measurements and instrumentations

NMR spectra were recorded on a JEOL JNM-AL 400 Fourier-transform NMR spectrometers (400 MHz). The chemical shifts of the ^{1}H, ^{13}C{^{1}H}, ^{11}B{^{1}H} and ^{19}F{^{1}H} NMR spectra determined in $CDCl_3$ were given in ppm relative to tetramethylsilane (0.00 ppm for ^{1}H and ^{13}C{^{1}H}) as an internal standard, or boron trifluoride diethyl-ether complex (0.00 ppm for ^{11}B{^{1}H}) and hexafluorobenzene (−164.9 ppm *vs.* $CFCl_3$ for ^{19}F{^{1}H}) as external standards. High-resolution fast-atom bombardment mass spectroscopies (HR-FAB-MS) were carried out on a JEOL JMS-700N spectrometer. Elemental analyses (C, H, N) were performed by a Perkin Elmer 2400II elemental analyzer. UV-vis absorption spectra were recorded on a Jasco V-560 spectrophotometer. The corrected emission spectra were obtained by using a Jasco F-6500 spectrofluorometer (excitation wavelength = 365 nm). Fluorescence decay measurements were conducted by using a Hamamatsu Photonics picosecond fluorescence lifetime measurement system C11200 equipped with picosecond light pulser PLP-10 as a 405 nm excitation light source. Emission quantum yields were determined by using a Hamamatsu Photonic Absolute PL Quantum Yield Measurement System C9920-02 (excitation wavelength = 365 nm). For the photophysical measurements, spectrophotometric-grade toluene was used as supplied.

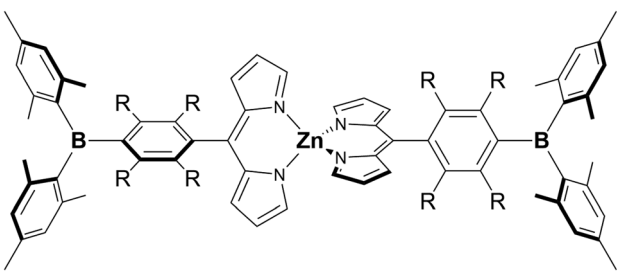

Chart 1 Chemical structures of **ZnBph** (R = H) and **ZnBdu** (R = CH_3).

Synthesis of (4-iodo-2,3,5,6-tetramethylphenyl)bis(2,4,6-trimethylphenyl)borane (1)

Synthesis was performed with minor changes in the reported procedures.[27] An oven-dried Schlenk tube was evacuated and filled subsequently with an argon gas. 1,4-Diiodo-2,3,5,6-tetramethylbenzene (2.8 g, 7.2 mmol) and dry diethyl ether (20 mL) was added, then, cooled to −78 °C in an acetone/dry-ice bath. *n*-Butyllithium in *n*-hexane (1.6 M, 5.2 mL, 8.3 mmol) was added to the reaction mixture at −78 °C. After stirring at −78 °C for 1 h, the reaction mixture became a pale-yellow suspension. Bis(2,4,6-trimethylphenyl)boron fluoride (2.1 g, 7.9 mmol) dissolved in dry diethyl ether (20 mL) was added to the reaction mixture, then, the mixture allowed to warm to room temperature and continuously stirred overnight. The reaction mixture became a yellow suspension. After an addition of HCl(aq) (1 M, 20 mL), the mixture was extracted with diethyl ether (30 mL × 2). The combined organic extract was washed with water (50 mL), dried over anhydrous Na_2SO_4 and concentrated under reduced pressure. The crude product was washed with *n*-hexane (50 mL) to give pure **1** (2.0 g, 59%) as a colorless solid. ^{1}H NMR (400 MHz, $CDCl_3$) δ: 6.73 (4H, s, *m*-Ar-H of mesityl), 2.43 (6H, s, 2,6-CH_3 of duryl), 2.26 (6H, s, *p*-CH_3 of mesityl), 2.09 (6H, s, 3,5-CH_3 of duryl), 1.94 ppm (12H, s, *o*-CH_3 of mesityl).

Synthesis of 4-[bis(2,4,6-trimethylphenyl)boryl]-2,3,5,6-tetramethylbenzaldehyde (2)

An oven-dried Schlenk tube was evacuated and filled subsequently with an argon gas. **1** (2.0 g, 4.9 mmol) and dry tetrahydrofuran (20 mL) was added, then, cooled to −78 °C in an acetone/dry-ice bath. *n*-Butyllithium in *n*-hexane (1.6 M, 4.4 mL, 7.0 mmol) was added to the reaction mixture at −78 °C. After stirring at −78 °C for 1 h, the reaction mixture became an orange suspension. Dry *N*,*N*-dimethylformamide (2.0 mL) was added to the reaction mixture at −78 °C. After stirring at −78 °C

for 1 h, the reaction mixture became a yellow solution. Then, HCl(aq) (1 M, 50 mL) was added and stirred for another 4 h. The reaction mixture was extracted with ethyl acetate (30 mL × 2). The combined organic extract was washed with water (50 mL), dried over anhydrous $MgSO_4$ and concentrated under reduced pressure. The crude product was purified by recrystallization from ethyl acetate to give pure **2** (1.3 g, 65%) as a pale-yellow solid. ^{1}H NMR (400 MHz, $CDCl_3$) δ: 10.7 (1H, s, CHO), 6.75 (4H, s, *m*-Ar-H of mesityl), 2.31 (6H, s, 2,6-CH_3 of duryl), 2.27 (6H, s, *p*-CH_3 of mesityl), 2.02 (6H, s, 3,5-CH_3 of duryl), 1.95 ppm (12H, s, *o*-CH_3 of mesityl).

Synthesis of 5-{4-[bis(2,4,6-trimethylphenyl)boryl]-2,3,5,6-tetramethylphenyl}dipyrrin (3)

2 (501.4 mg, 1.22 mmol) was dissolved in neat pyrrole (25 mL) and degassed by a nitrogen-gas bubbling for 30 min. Trifluoroacetic acid (20 μL, 0.23 mmol) was then added, and stirred at room temperature for 10 min. The reaction mixture was diluted with CH_2Cl_2 (50 mL), washed with NaOH(aq) (1 M, 50 mL) and dried over anhydrous $MgSO_4$. After removing $MgSO_4$ by filtration and evaporation of CH_2Cl_2 under reduced pressure, the remaining pyrrole was removed by vacuum distillation with heating (40 °C). Then, the product was added to a solution of *p*-chloranil (500 mg, 2.04 mmol) in CH_2Cl_2 (50 mL). The solution color changed from yellow to dark yellow-green. The solution was stirred overnight and, then, filtered and evaporated to remove resultant insolubles and CH_2Cl_2 respectively. The reaction mixture was processed by reprecipitation (CH_2Cl_2/*n*-hexane) and silica-gel column chromatography, eluting with CH_2Cl_2, to give the pure product (125 mg, 20%) as a pale yellow-green solid. ^{1}H NMR (400 MHz, $CDCl_3$) δ: 7.66 (2H, s, 1,9-Ar-H of dipyrrin), 6.78 (4H, s, *m*-Ar-H of mesityl), 6.39 (2H, dd, J = 1.1, 4.1 Hz, 2,8-Ar-H of dipyrrin), 6.36 (2H, dd, J = 1.6, 3.8 Hz, 3,7-Ar-H of dipyrrin), 2.29 (6H, s, *p*-CH_3 of mesityl), 2.05 (6H, s, 3,5-CH_3 of durylene), 2.01 (12H, d, J = 7.9 Hz, *o*-CH_3 of mesityl), 1.94 ppm (6H, s, 2,6-CH_3 of durylene). FAB-MS (CH_2Cl_2) *m*/*z*: 525 ($[M + H]^+$).

Synthesis of bis(5-{4-[bis(2,4,6-trimethylphenyl)boryl]phenyl}dipyrrinato)zinc(II) (ZnBph)

To a CH_2Cl_2 solution (50 mL) of 5-{4-[bis(2,4,6-trimethylphenyl)boryl]phenyl}dipyrrin (100 mg, 0.21 mmol), a CH_3OH solution (10 mL) of $Zn(OAc)_2 \cdot 2H_2O$ (138 mg, 0.63 mmol) was added and stirred at room temperature. After stirring overnight, the solvent was evaporated under reduced pressure. The crude product was purified by silica-gel column chromatography, eluting with CH_2Cl_2. Recrystallization from CH_2Cl_2/methanol afforded pure **ZnBph** (98.5 mg, 45%) as an orange solid. ^{1}H NMR (400 MHz, $CDCl_3$) δ: 7.60 (4H, d, J = 7.6 Hz, 2,6-Ar-H of phenylene), 7.55 (4H, d, J = 6.9 Hz, 3,5-Ar-H of phenylene), 7.54 (4H, s, 1,9-Ar-H of dipyrrinate), 6.86 (8H, s, *m*-Ar-H of mesityl), 6.68 (4H, d, J = 3.8 Hz, 2,8-Ar-H of dipyrrinate), 6.38 (4H, d, J = 3.8 Hz, 3,7-Ar-H of dipyrrinate), 2.33 (12H, s, *p*-CH_3 of mesityl), 2.02 ppm (24H, s, *o*-CH_3 of mesityl). ^{13}C{^{1}H} NMR ($CDCl_3$) δ: 149.9, 148.6, 146.4, 142.3, 141.8, 140.9, 140.3, 139.0, 134.8, 132.8, 130.4, 128.3, 117.2, 23.5, 21.3 ppm. ^{11}B{^{1}H} NMR ($CDCl_3$) δ: 75.7 ppm. HR-FAB-MS (CH_2Cl_2) *m*/*z*: calculated for $C_{66}H_{65}B_2N_4Zn^+$ ($[M + H]^+$), 999.4687; found, 999.4687. Anal. calcd (%) for $C_{66}H_{64}B_2N_4Zn \cdot CH_3OH$: C, 77.96; H, 6.64; N, 5.43. Found: C, 77.61; H, 6.63; N, 5.31.

Synthesis of bis(5-{4-[bis(2,4,6-trimethylphenyl)boryl]-2,3,5,6-tetramethylphenyl}dipyrrinato)zinc(II) (ZnBdu)

To a CH_2Cl_2 solution (30 mL) of **3** (125 mg, 0.24 mmol), a CH_3OH solution (10 mL) of $Zn(OAc)_2 \cdot 2H_2O$ (158 mg, 0.72 mmol) was added and stirred at room temperature. After stirring overnight, the solvent was evaporated under reduced pressure. The crude product was purified by silica-gel column chromatography, eluting with CH_2Cl_2. Recrystallization from CH_2Cl_2/methanol afforded pure **ZnBdu** (80.8 mg, 61%) as a yellow-brown solid. ^{1}H NMR (400 MHz, $CDCl_3$) δ: 7.50 (4H, s, 1,9-Ar-H of dipyrrinate), 6.79 (8H, d, J = 6.8 Hz, *m*-Ar-H of mesityl), 6.57 (4H, d, J = 4.0 Hz, 2,8-Ar-H of dipyrrinate), 6.38 (4H, d, J = 4.2 Hz, 3,7-Ar-H of dipyrrinate), 2.30 (12H, s, *p*-CH_3 of mesityl), 2.10 (12H, s, 2,6-CH_3 of durylene), 2.05 (12H, s, 3,5-CH_3 of durylene), 2.02 ppm (24H, s, *o*-CH_3 of *o*-mesityl). ^{13}C{^{1}H} NMR ($CDCl_3$) δ: 150.3, 149.0, 144.6, 141.0, 140.8, 140.3, 139.4, 138.9, 134.9, 132.1, 131.3, 129.0, 128.8, 117.0, 29.7, 23.3, 22.9, 21.2, 19.9, 17.4 ppm. ^{11}B{^{1}H} NMR ($CDCl_3$) δ: 79.8 ppm. HR-FAB-MS (CH_2Cl_2) *m*/*z*: calculated for $C_{74}H_{81}B_2N_4Zn^+$ ($[M + H]^+$), 1111.5939; found, 1111.5938. Anal. calcd (%) for $C_{74}H_{80}B_2N_4Zn \cdot CH_3OH$: C, 78.71; H, 7.40; N, 4.90. Found: C, 78.89; H, 7.35; N, 4.77.

X-ray crystal structure determinations

Diffraction data were collected at −180 °C under a steam of cold N_2 gas on a Rigaku RA-Micro7 HFM instrument equipped with a Rigaku Saturn724+ CCD detector by using graphite-monochromated Mo Kα radiation. The frame data were integrated using a Rigaku CrystalClear program package,[65] and the data sets were corrected for absorption using a REQAB program. The calculation was performed with a CrystalStructure software package[66] except for refinement, which was performed using SHELXL Version 2018/3.[67] The structures were solved by direct methods and refined on F^2 by the full-matrix least-squares methods. Anisotropic refinement was applied to all non-hydrogen atoms with the exception of the crystal solvents. All hydrogen atoms were put at calculated positions.

Computational methods

Theoretical calculations for the complexes were conducted with Gaussian 16W software (Revision A.03).[68] Optimizations of the ground-state geometries of the complexes were performed by using the B3LYP density functional theory (DFT).[69,70] The LanL2DZ[71–73] and 6-31G(d,p)[74] basis sets were used to treat the geometrical structures of the zinc and all other atoms, respectively. Time-dependent DFT (TD-DFT) calculations were then performed to estimate the energies and oscillator strengths *f* of electronic excitation transitions generating the 50 lowest-energy singlet excited states. All of the calculations were carried out as in toluene by using a polarizable continuum model (PCM).[75] Optimized geometries, Kohn–Sham molecular orbitals and

natural transition orbitals (isovalue = 0.03 e Å^{-3}) were visualized by GaussView 5.[76]

Results and discussion

Synthesis and characterization

Novel dipyrrinato zinc(II) complexes **ZnBph** and **ZnBdu** were successfully synthesized in moderate yields (45% for **ZnBph**, 61% for **ZnBdu**) by mixing $Zn(OAc)_2 \cdot 2H_2O$ and relevant dipyrrin in a dichloromethane/methanol mixture at room temperature. The complexes were identified by the ^{1}H and $^{13}C\{^1H\}$ NMR spectroscopies, HR-FAB-MS and elemental analysis. In the ^{1}H NMR spectra of **ZnBph** and **ZnBdu** (see Fig. S3 and S4†), four protons at 1- and 9-positions of dipyrrinate moiety were observed as singlet at 7.50–7.54 ppm which was shifted to upfield upon the complexation. Two doublets ascribed to protons at 2,8- and 3,7-positions were observed at 6.38–6.68 ppm. The trends are similar to other bis(dipyrrinato)zinc(II) complexes.[54] Single crystals of **ZnBdu** suitable for X-ray crystallographic analysis were obtained from CH_2Cl_2/*n*-pentane. The X-ray structure of **ZnBdu** is shown in Fig. 1(a), whose crystallographic data is summarized in Table S1.† The zinc center takes a tetrahedral geometry with a dihedral angle for two Zn–N_2(dipyrrinato) planes being 90°. The distance between the zinc center and each pyrrolic nitrogen is 1.983 Å, which are similar to those in **Znph** (1.973–1.988 Å).[54] The dihedral angle between a dipyrrinato ligating and bridging durylene moieties was 77.9°. The value is similar to those of the previous iridium(III)[41] (71.1°) and platinum(II) complexes (80.7° and 68.7°).[42] The boron atoms in the arylborane groups take a planar sp^2-like configuration with B–C bond lengths being 1.57–1.58 Å and C–B–C angles being ~120°. Dihedral angle between the durylene and BC_3 plane was 54.1°. These structural characteristics of **ZnBdu** in the crystalline phase are indicative of the conjugation between the dipyrrinate moiety and boron atom in the ligand. The structures of the complexes were compared on the basis of the DFT calculations because single crystals of **ZnBph** suitable for X-ray structural analysis were not obtained in spite of many efforts for recrystallization from various conditions. Optimized geometries of **ZnBph** and **ZnBdu** are shown in Fig. 1(b) and (c), respectively. The zinc centers in both complexes take tetrahedral geometries, and zinc–nitrogen distances are in the range of 2.059–2.063 Å. The dihedral angle between dipyrrinato ligating moiety and bridging phenylene group (θ_1) in **ZnBph** (64.1°–64.3°) is smaller than that in **ZnBdu** (89.0–89.2°). Similar tendency was also observed for the tilt angle between arylene group and the BC_3 plane in the arylborane moiety (θ_2 = 21.7°–25.6° and 57.1°–57.7° for **ZnBph** and **ZnBdu**, respectively). On the basis of these angles, (cos θ_1 × cos θ_2) values as measures of the conjugation between the π

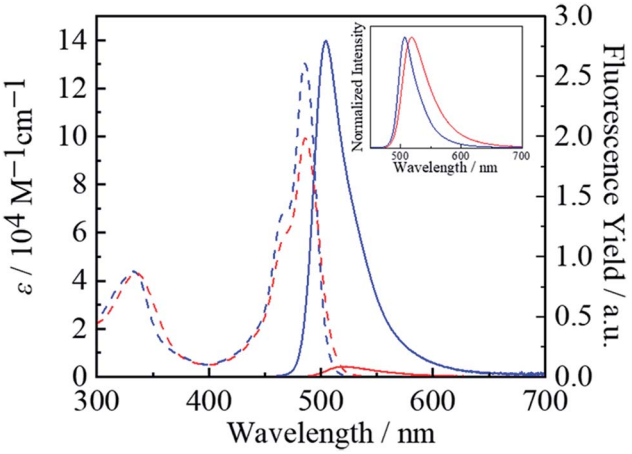

Fig. 2 UV-vis absorption (broken lines) and fluorescence spectra (solid lines) of **ZnBph** (red) and **ZnBdu** (blue) in toluene at 298 K. The integrations of the fluorescence spectra in a wavenumber scale correspond relatively to the fluorescence quantum yields of the complexes. Inset: normalized fluorescence spectra.

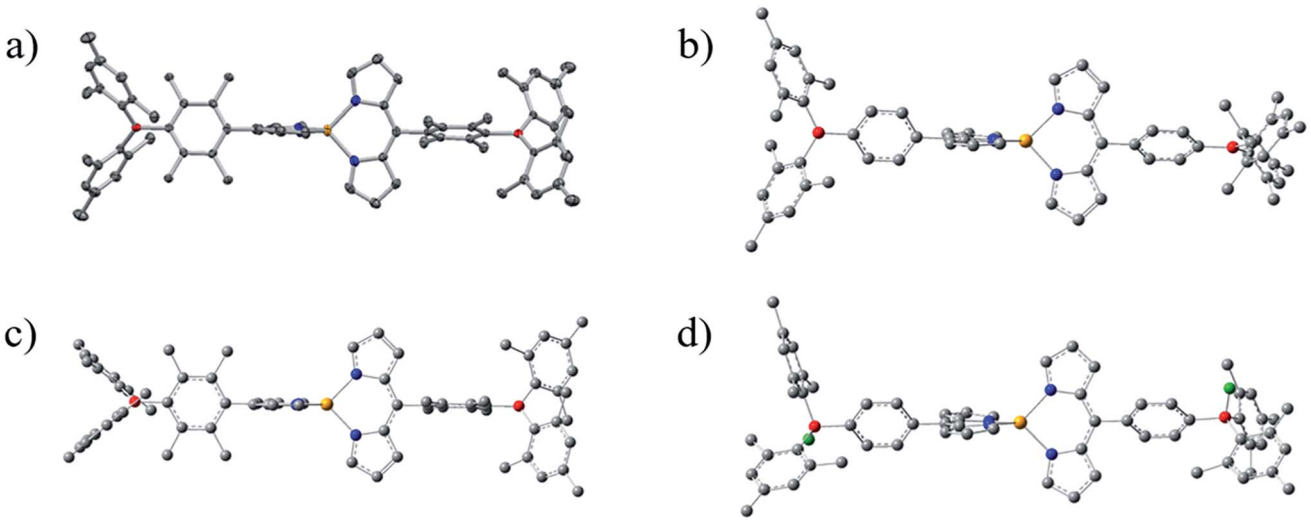

Fig. 1 Perspective view of crystal structure for **ZnBdu** ((a) 50% probability ellipsoids) and DFT optimized geometries of **ZnBph** (b), **ZnBdu** (c) and **ZnBph**·2F$^-$ (d): carbon (gray), nitrogen (blue), boron (red), zinc (orange) and fluorine (green). Hydrogen atoms are omitted for clarity.

Table 1 Spectroscopic and photophysical properties of the dipyrrinato zinc(II) complexes in toluene at 298 K

Complex	λ_{abs}/nm (ε/10^4 M^{-1} cm^{-1})	λ_f/nm	Φ_f	τ_f/ns	$k_r{}^a$/s^{-1}	$k_{nr}{}^a$/s^{-1}
ZnBph	334 (4.3), 487 (09.2)	517	0.01	1.3	7.7×10^6	7.6×10^8
ZnBdu	333 (4.4), 486 (13.2)	504	0.34	2.7	1.3×10^8	2.4×10^8
ZnBph·2F$^-$	383 (1.6), 481 (09.4)	503	0.02	0.2	1×10^8	5×10^9
Znph[b]	485	500	0.006	0.09	7×10^7	1×10^{10}
Znph[c]	322 (1.4), 482 (11.5)	500				
Znmes[b]	487	501	0.36	2.7	1.3×10^8	2.4×10^8
Znmes[c]	345, 485	501				

[a] Calculated by the equation, $\Phi_f = k_r/(k_r + k_{nr}) = k_r\tau_f$. [b] Data in toluene compiled from ref. 62. [c] Data in CH_2Cl_2 compiled from ref. 54.

orbital of the dipyrrinate moiety and the vacant p orbital on the boron atom *via* the bridging arylene moiety in **ZnBph** and **ZnBdu** were calculated to be 40 and 1%, respectively. The smaller dihedral angle in **ZnBph** than in **ZnBdu** strongly indicates enhanced electronic interactions between the dipyrrinato zinc(II) complex and the arylborane moieties, and therefore larger contribution of the arylborane moieties to the spectroscopic/photophysical properties of a complex are expected.

Absorption spectra

Fig. 2 shows absorption spectra of **ZnBph** and **ZnBdu** in toluene at 298 K, and the spectroscopic properties are summarized in Table 1. The complexes exhibited intense/narrow and weak/broad absorption bands at around 487 and 334 nm, respectively. According to the DFT calculations (*vide infra*), the former band is assigned to the typical $\pi\pi^*$ transitions in a dipyrrinato ligand and the latter is ascribed to π(aryl)–p(B) CT transitions in an arylborane moiety, similarly to other arylborane–dipyrrinato metal complexes.[41,42] The absorption maximum wavelengths of **ZnBph** and **ZnBdu** (λ_{abs} = 487 and 486 nm, respectively) are comparable with those of **Znph** and **Znmes** (λ_{abs} = 485 nm and 487 nm, respectively) without any arylborane substituents.[62] Interestingly, the molar absorption coefficients (ε) at the maximum wavelength (λ_{abs}) of the low-energy band of the complexes (9.2×10^4 M^{-1} cm^{-1} for **ZnBph** and 1.32×10^5 M^{-1} cm^{-1} for **ZnBdu**) were larger than those of the arylborane–dipyrrinato iridium(III) and platinum(II) complexes (ε = 7.4×10^4 and 2.2×10^4 M^{-1} cm^{-1}, respectively)[41,42] whose $\pi\pi^*$

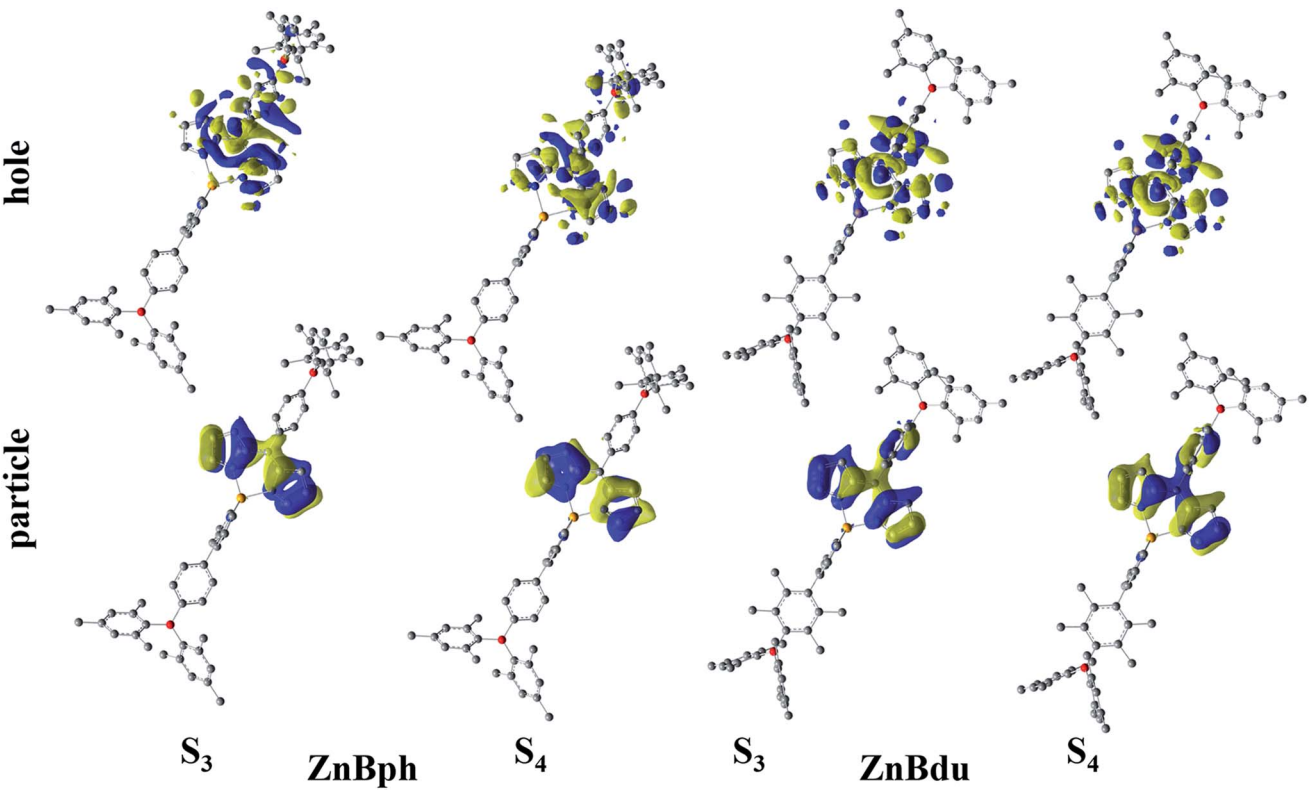

Fig. 3 NTOs for S_3 and S_4 states of the complexes in toluene. Hydrogen atoms are omitted for clarity.

Chart 2 Structural change of an arylborane compound upon the binding of fluoride.

transitions synergistically interact with MLCT and/or π(aryl)–p(B) CT ones. Such differences in the ε values indicates that an introduction of the charge-transfer character to the ππ* transition in a dipyrrinato–metal complex decreases the relevant oscillator strength. Thus, smaller ε value of **ZnBph** suggests the existence of the π interactions throughout the ligand presumably owing to the smaller dihedral angles between dipyrrinate–phenylene and phenylene–dimesitylboryl moieties. These discussions were theoretically supported by TD-DFT calculations as summarized in Tables S2–S5.† For both complexes, intense absorption bands at ~487 nm appeared as electronic transitions generating third (S_3) and forth excited states (S_4). Fig. 3 shows natural transition orbitals (NTOs) for the S_3 and S_4 states of the complexes. Both S_3 and S_4 states of **ZnBph** originate in electronic transitions from the dipyrrinate moiety to the whole ligand, gaining the π(aryl)–p(B) CT character, whereas those of **ZnBdu** are assignable to the pure ππ* transitions in a 5-duryldipyrrinate moiety.

Fluorescence spectra and photophysical properties

As shown in Fig. 2, the fluorescence from **ZnBph** ($\Phi_f = 0.01$ in toluene at 298 K) was significantly weak compared with that from **ZnBdu** ($\Phi_f = 0.34$). Furthermore, the fluorescence spectrum of **ZnBph** (maximum wavelength $\lambda_f = 517$ nm) was broadened and shifted to lower-energy compared with those of **ZnBdu** (504 nm), **Znph** (501 nm)[62] and **Znmes** (500 nm)[62] see Table 1. The spectroscopic data of **ZnBph** indicate a partial contribution of a CT character arising from the low-energy p(B) to the fluorescent excited state and energetic stabilization of the excited state by the solvation. In practice, the radiative rate constant (k_r) of **ZnBph** (7.7×10^6 s^{-1}, see Table 1) was 17-times smaller than that of **ZnBdu** (1.3×10^8 s^{-1}) owing to a decreased wavefunction overlap between the excited and ground states.

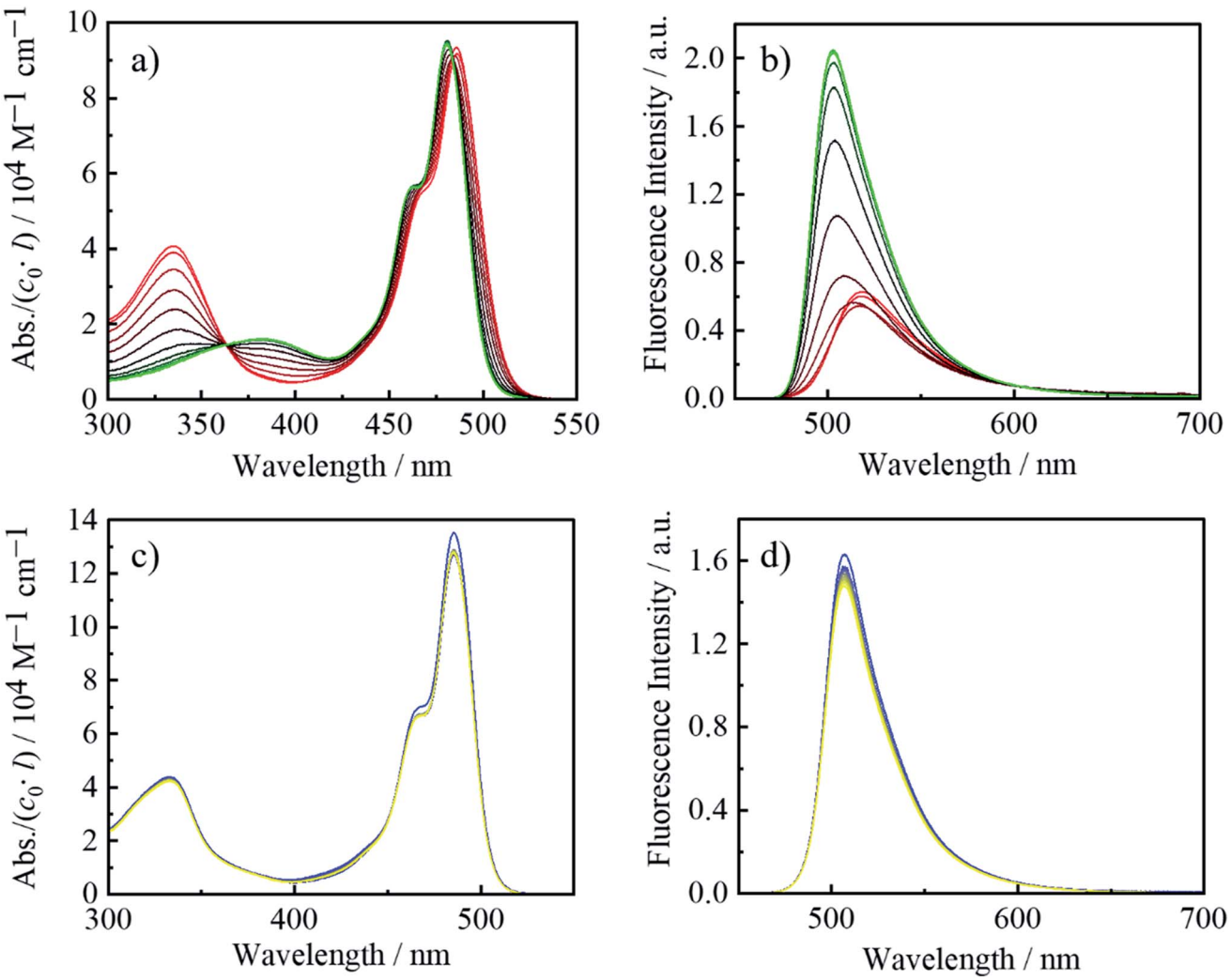

Fig. 4 UV-vis absorption and fluorescence spectral changes upon an addition of TBAF (0–4.0 equiv.) in toluene: **ZnBph** ((a and b) red to green) and **ZnBdu** ((c and d) blue to yellow).

Furthermore, the CT character in the excited state accelerated thermal deactivation to the ground state as the nonradiative decay rate constant (k_{nr}) of **ZnBph** (7.6×10^8 s^{-1}) was three-times larger than that of **ZnBdu** ($k_{nr} = 2.4 \times 10^8$ s^{-1}). It should be noted that the k_r and k_{nr} values of **ZnBdu** are comparable to those of **Znmes** ($k_r = 1.3 \times 10^8$ s^{-1} and $k_{nr} = 2.4 \times 10^8$ s^{-1}).[54] Thus, the strong fluorescence from **ZnBdu** would originate in the pure ππ* excited state and suppressed non-radiative decay processes owing to the presence of the bulky durylene bridging units. On the other hand, the k_r and k_{nr} values of **ZnBph** are significantly smaller than those of **Znph** ($k_r = 7 \times 10^7$ s^{-1} and $k_{nr} = 1 \times 10^{10}$ s^{-1}),[54] suggesting the existence of CT interactions in the excited state. As results, the fluorescence from **ZnBph** was well characterized by the ππ*/ILCT excited state, and the participation of the ILCT character in the excited state of a complex was revealed by varying the extent of π-conjugation between the dipyrrinate and arylborane moieties.

Spectroscopic responses to fluoride

Since the electron-deficient boron atom in an arylborane derivative can bind with a small Lewis base such as fluoride (Chart 2) with a binding constant being $\sim 10^6$ M^{-1},[77,78] we carried out the fluoride-addition experiments for the complexes. Fig. 4 shows absorption and fluorescence spectra of the complexes in the absence and presence of tetra-*n*-butylammonium fluoride (TBAF) in toluene. The absorbances of each spectrum were divided by the total concentration of the complex (c_0) and optical path length (l) so that the vertical axis corresponds to the molar absorption coefficient. Upon an addition of TBAF to **ZnBph**, the π(aryl)–p(B) CT absorption band at around 334 nm disappeared, and a broad absorption band at around 383 nm appeared with an isosbestic point at 360 nm. In addition, the fluoride binding shortened the maximum wavelength of the lowest-energy ππ*/ILCT absorption band of **ZnBph** from 487 nm to 481 nm, similarly to that observed for the relevant cyclometalated iridium(III) complex.[41] Complete disappearance of the π(aryl)–p(B) CT band and the complicated spectral changes in the absorption band at ~480 nm indicate successive bindings of two fluoride, affording a 1 : 1 adduct, followed by a 1 : 2 adduct, **ZnBph**·**2F**$^-$. The spectroscopic changes arising from the binding of fluoride to the boron atom were strongly evidenced by ^{1}H, ^{11}B{^{1}H} and ^{19}F{^{1}H} NMR measurements as shown in Fig. S8, S10 and S13,† respectively. The ^{11}B NMR signal of **ZnBph** was drastically shifted from 75.7 ppm to 5.5 ppm upon the addition of fluoride as TBAF. The broad signal was also observed at −174.41 ppm for the ^{19}F NMR spectrum of **ZnBph** in the presence of TBAF (4.0 eq.) owing to the coupling to ^{10}B ($I = 3$) and ^{11}B ($I = 3/2$), indicating the formation of B–F bond with **ZnBph**. In addition, the absence of the signal at −84.04 ppm (corresponding to the signal of $CDClF_2$ generated by the reaction of fluoride with solvent molecule $CDCl_3$)[79] in the ^{19}F NMR spectrum of **ZnBph** suggests that fluoride quickly binds to the boron atom before proceeding the exchange reaction of fluoride with chloride in the solvent molecule. Consequently, the binding of fluoride to the boron atom in **ZnBph** increased electron density around the boron atom.

The structure of **ZnBph**·**2F**$^-$ was theoretically investigated by the DFT calculation and the optimized geometry is shown in Fig. 1(d). Each boron atom possesses a tetrahedral geometry, and the dihedral angles between a dipyrrinato ligating moiety and bridging phenylene group (θ_1) were reduced to be 56.8°–58.7°. The structural and electronic changes increased the transition energy of the lowest-energy absorption band through efficient electron donation from the fluorinated arylborane group to the dipyrrinato moiety, leading to the decrease of electron density on the dipyrrinato moiety and therefore the downfield-shift of proton signals in the pyrrole rings (see Fig. S15† for HOMO and HOMO−1). The fluorescence from **ZnBph** was shifted to higher-energy with a slight decrease in intensity and then enhanced largely upon a continuous addition of TBAF as shown in Fig. 4(b). The maximum wavelength ($\lambda_f = 503$ nm) and band shape in the presence of ≥3.0 equivalence of fluoride were almost identical to those of **ZnBdu**, and the k_r value of **ZnBph**·**2F**$^-$ (1×10^8 s^{-1}) was also similar to that of **ZnBdu**. Owing to these fluorescence characteristics, it can be expected that the fluorescent excited state of **ZnBph**·**2F**$^-$ possesses the pure ππ* character. Significantly smaller Φ_f (0.02) of **ZnBph**·**2F**$^-$ than that of **ZnBdu** can be explained by enhanced thermal deactivation ($k_{nr} = 5 \times 10^9$ s^{-1}) *via* a rotation of the phenylene moiety as reported for **Znph** and **Znmes** ($k_{nr} = 1.1 \times 10^{10}$ and 3.2×10^8 s^{-1} in toluene, respectively).[54] On the other hand, there was no experimental evidence of the fluoride binding to **ZnBdu** in the absorption, fluorescence and ^{1}H, ^{11}B{^{1}H} and ^{17}F{^{1}H} NMR spectra as shown in Fig. 4(c) and (d), S9, S11 and S14† presumably due to the steric hindrance of the durylene moieties. Thus, fluoride binding affinity of an arylborane–dipyrrinato zinc(II) complex was controllable by the bridging arylene moiety and, upon the fluoride binding, the excited-state electronic structure of **ZnBph** was switched from ππ*/ILCT to pure ππ*.

Conclusions

The bridging arylene moieties in novel bis(dipyrrinato)zinc(II) derivatives having the arylborane groups at 5-position of the dipyrrinato ligands had significant impacts on the absorption/fluorescence spectra and fluoride-binding affinity of the complex. The theoretical calculations suggest that **ZnBph** with the phenylene linkers possesses smaller dihedral angles between dipyrrinate–phenylene and phenylene–dimesitylboryl moieties than the relevant values of **ZnBdu** with the durylene linkers. The smaller dihedral angles in **ZnBph** afford the π-conjugation in the entire of the ligand and, therefore, the electron-withdrawing arylborane groups participate in the electronic structure of the complex. As a result, the excited state of **ZnBph** was best characterized by the synergistic ππ*/ILCT, whereas that of **ZnBdu** was the pure ππ*. **ZnBph** could bind with fluoride, and the excited state was switched from ππ*/ILCT to pure ππ* upon the fluoride binding owing to the disappearance of the electron-withdrawing ability of the dimesitylboryl moieties. Thus, we revealed the importance of the

molecular design including the linker structure in metal complexes with an arylborane group(s). Tuning of the extent of the CT character in an excited-state metal complex will be an important factor to control spectroscopic and photophysical properties of metal complexes.

Conflicts of interest

The authors declare no competing financial interest.

Acknowledgements

This research was partially funded by the Sasakawa Scientific Research Grant from the Japan Science Society. We are grateful to J. Nagaoka for the technical assistance and the X-ray measurements.

References

1 C. D. Entwistle and T. B. Marder, *Chem. Mater.*, 2004, **16**, 4574–4585.
2 L. Ji, S. Griesbeck and T. B. Marder, *Chem. Sci.*, 2017, **8**, 846–863.
3 S. Y. Li, Z. B. Sun and C. H. Zhao, *Inorg. Chem.*, 2017, **56**, 8705–8717.
4 Z. M. Hudson and S. Wang, *Acc. Chem. Res.*, 2009, **42**, 1584–1596.
5 R. Misra, T. Jadhav, B. Dhokale and S. M. Mobin, *Dalton Trans.*, 2015, **44**, 16052–16060.
6 S. Yamaguchi, S. Akiyama and K. Tamao, *J. Am. Chem. Soc.*, 2000, **122**, 6335–6336.
7 S. Yamaguchi, T. Shirasaka and K. Tamao, *Org. Lett.*, 2000, **2**, 4129–4132.
8 A. Ito, T. Hiokawa, E. Sakuda and N. Kitamura, *Chem. Lett.*, 2010, **40**, 34–36.
9 N. Kitamura and E. Sakuda, *J. Phys. Chem. A*, 2005, **109**, 7429–7434.
10 N. Kitamura, E. Sakuda, T. Yoshizawa, T. Iimori and N. Ohta, *J. Phys. Chem. A*, 2005, **109**, 7435–7441.
11 E. Sakuda, K. Tsuge, Y. Sasaki and N. Kitamura, *J. Phys. Chem. B*, 2005, **109**, 22326–22331.
12 E. Sakuda, A. Funahashi and N. Kitamura, *Inorg. Chem.*, 2006, **45**, 10670–10677.
13 Y. Sun, N. Ross, S. Bin Zhao, K. Huszarik, W. L. Jia, R. Y. Wang, D. Macartney and S. Wang, *J. Am. Chem. Soc.*, 2007, **129**, 7510–7511.
14 S. Bin Zhao, T. McCormick and S. Wang, *Inorg. Chem.*, 2007, **46**, 10965–10967.
15 G. Zhou, C. L. Ho, W. Y. Wong, Q. Wang, D. Ma, L. Wang, Z. Lin, T. B. Marder and A. Beeby, *Adv. Funct. Mater.*, 2008, **18**, 499–511.
16 N. You and S. Y. Park, *Adv. Mater.*, 2008, **20**, 3820–3826.
17 Q. Zhao, F. Li, S. Liu, M. Yu, Z. Liu, T. Yi and C. Huang, *Inorg. Chem.*, 2008, **47**, 9256–9264.
18 Y. L. Rao and S. Wang, *Inorg. Chem.*, 2009, **48**, 7698–7713.
19 Z. M. Hudson, S. Bin Zhao, R. Y. Wang and S. Wang, *Chem.–Eur. J.*, 2009, **15**, 6131–6137.
20 S. T. Lam, N. Zhu and V. W. W. Yam, *Inorg. Chem.*, 2009, **48**, 9664–9670.
21 W. J. Xu, S. J. Liu, X. Y. Zhao, S. Sun, S. Cheng, T. C. Ma, H. Bin Sun, Q. Zhao and W. Huang, *Chem.–Eur. J.*, 2010, **16**, 7125–7133.
22 C. R. Wade and F. P. Gabbai, *Inorg. Chem.*, 2010, **49**, 714–720.
23 E. Sakuda, Y. Ando, A. Ito and N. Kitamura, *Inorg. Chem.*, 2011, **50**, 1603–1613.
24 A. Ito, T. Hiokawa, E. Sakuda and N. Kitamura, *Chem. Lett.*, 2010, **40**, 34–36.
25 Z. M. Hudson and S. Wang, *Organometallics*, 2011, **30**, 4695–4701.
26 Y. Sun, Z. M. Hudson, Y. Rao and S. Wang, *Inorg. Chem.*, 2011, **50**, 3373–3378.
27 A. Ito, Y. Kang, S. Saito, E. Sakuda and N. Kitamura, *Inorg. Chem.*, 2012, **51**, 7722–7732.
28 Z. M. Hudson, C. Sun, M. G. Helander, Y. L. Chang, Z. H. Lu and S. Wang, *J. Am. Chem. Soc.*, 2012, **134**, 13930–13933.
29 R. S. Vadavi, H. Kim, K. M. Lee, T. Kim, J. Lee, Y. S. Lee and M. H. Lee, *Organometallics*, 2012, **31**, 31–34.
30 S. B. Ko, J. S. Lu, Y. Kang and S. Wang, *Organometallics*, 2013, **32**, 599–608.
31 N. Wang, S. B. Ko, J. S. Lu, L. D. Chen and S. Wang, *Chem.–Eur. J.*, 2013, **19**, 5314–5323.
32 X. Wang, Y. L. Chang, J. S. Lu, T. Zhang, Z. H. Lu and S. Wang, *Adv. Funct. Mater.*, 2014, **24**, 1911–1927.
33 S. Sharma, H. Kim, Y. H. Lee, T. Kim, Y. S. Lee and M. H. Lee, *Inorg. Chem.*, 2014, **53**, 8672–8680.
34 Y. H. Lee, N. Van Nghia, M. J. Go, J. Lee, S. U. Lee and M. H. Lee, *Organometallics*, 2014, **33**, 753–762.
35 A. Nakagawa, E. Sakuda, A. Ito and N. Kitamura, *Inorg. Chem.*, 2015, **54**, 10287–10295.
36 A. Nakagawa, A. Ito, E. Sakuda, S. Fujii and N. Kitamura, *Eur. J. Inorg. Chem.*, 2017, 3794–3798.
37 N. Wang, M. Hu, S. K. Mellerup, X. Wang, F. Sauriol, T. Peng and S. Wang, *Inorg. Chem.*, 2017, **56**, 12783–12794.
38 L. F. Smith, B. A. Blight, H. J. Park and S. Wang, *Inorg. Chem.*, 2014, **53**, 8036–8044.
39 H. J. Park, S. B. Ko, I. W. Wyman and S. Wang, *Inorg. Chem.*, 2014, **53**, 9751–9760.
40 G. Rajendra Kumar and P. Thilagar, *Inorg. Chem.*, 2016, **55**, 12220–12229.
41 K. Takaki, E. Sakuda, A. Ito, S. Horiuchi, Y. Arikawa and K. Umakoshi, *Inorg. Chem.*, 2019, **58**, 14542–14550.
42 K. Takaki, E. Sakuda, A. Ito, S. Horiuchi, Y. Arikawa and K. Umakoshi, *Chem. Lett.*, 2020, **49**, 905–908.
43 T. E. Wood and A. Thompson, *Chem. Rev.*, 2007, **107**, 1831–1861.
44 Y. Wang, Z. Xue, Y. Dong and W. Zhu, *Polyhedron*, 2015, **102**, 578–582.
45 K. Servaty, E. Cauët, F. Thomas, J. Lambermont, P. Gerbaux, J. De Winter, M. Ovaere, L. Volker, N. Vaeck, L. Van Meervelt, W. Dehaen, C. Moucheron and A. Kirsch-De Mesmaeker, *Dalton Trans.*, 2013, **42**, 14188–14199.
46 T. M. McLean, D. M. Cleland, S. J. Lind, K. C. Gordon, S. G. Telfer and M. R. Waterland, *Chem.–Asian J.*, 2010, **5**, 2036–2046.

47 E. Zeini Jahromi and J. Gailer, *Dalton Trans.*, 2010, **39**, 329–336.
48 S. Riese, M. Holzapfel, A. Schmiedel, I. Gert, D. Schmidt, F. Würthner and C. Lambert, *Inorg. Chem.*, 2018, **57**, 12480–12488.
49 T. M. McLean, J. L. Moody, M. R. Waterland and S. G. Telfer, *Inorg. Chem.*, 2012, **51**, 446–455.
50 C. Bronner, M. Veiga, A. Guenet, L. De Cola, M. W. Hosseini, C. A. Strassert and S. A. Baudron, *Chem.–Eur. J.*, 2012, **18**, 4041–4050.
51 C. Bronner, S. A. Baudron, M. W. Hosseini, C. A. Strassert, A. Guenet and L. De Cola, *Dalton Trans.*, 2010, **39**, 180–184.
52 K. Hanson, A. Tamayo, V. V. Diev, M. T. Whited, P. I. Djurovich and M. E. Thompson, *Inorg. Chem.*, 2010, **49**, 6077–6084.
53 M. A. Filatov, A. Y. Lebedev, S. N. Mukhin, S. A. Vinogradov and A. V. Cheprakov, *J. Am. Chem. Soc.*, 2010, **132**, 9552–9554.
54 L. Yu, K. Muthukumaran, I. V. Sazanovich, C. Kirmaier, E. Hindin, J. R. Diers, P. D. Boyle, D. F. Bocian, D. Holten and J. S. Lindsey, *Inorg. Chem.*, 2003, **42**, 6629–6647.
55 M. Asaoka, Y. Kitagawa, R. Teramoto, K. Miyagi, Y. Natori, R. Sakamoto, H. Nishihara and M. Nakano, *Polyhedron*, 2017, **136**, 113–116.
56 R. Matsuoka, R. Toyoda, R. Sakamoto, M. Tsuchiya, K. Hoshiko, T. Nagayama, Y. Nonoguchi, K. Sugimoto, E. Nishibori, T. Kawai and H. Nishihara, *Chem. Sci.*, 2015, **6**, 2853–2858.
57 M. Tsuchiya, R. Sakamoto, M. Shimada, Y. Yamanoi, Y. Hattori, K. Sugimoto, E. Nishibori and H. Nishihara, *Inorg. Chem.*, 2016, **55**, 5732–5734.
58 S. Kusaka, R. Sakamoto, Y. Kitagawa, M. Okumura and H. Nishihara, *Chem.–Asian J.*, 2012, **7**, 907–910.
59 R. Sakamoto, T. Iwashima, J. F. Kögel, S. Kusaka, M. Tsuchiya, Y. Kitagawa and H. Nishihara, *J. Am. Chem. Soc.*, 2016, **138**, 5666–5677.
60 D. Tungulin, J. Leier, A. B. Carter, A. K. Powell, R. Q. Albuquerque, A. N. Unterreiner and C. Bizzarri, *Chem.–Eur. J.*, 2019, **25**, 3816–3827.
61 Q. Jiang, N. Desbois, S. Wang and C. P. Gros, *J. Porphyrins Phthalocyanines*, 2020, **24**, 646–661.
62 I. V. Sazanovich, C. Kirmaier, E. Hindin, L. Yu, D. F. Bocian, J. S. Lindsey and D. Holten, *J. Am. Chem. Soc.*, 2004, **126**, 2664–2665.
63 C. Trinh, K. Kirlikovali, S. Das, M. E. Ener, H. B. Gray, P. Djurovich, S. E. Bradforth and M. E. Thompson, *J. Phys. Chem. C*, 2014, **118**, 21834–21845.
64 N. Z. Alqahtani, T. G. Blevins and C. E. McCusker, *J. Phys. Chem. A*, 2019, **123**, 10011–10018.
65 *CrystalClear: Data Collection and Processing Software*, Rigaku Corporation, Tokyo, Japan, 1998–2015.
66 *CrystalStructure 4.3: Crystal Structure Analysis Package*, Rigaku Corporation, Tokyo, Japan, 2000–2019.
67 SHELXL Version 2018/3:G. M. Sheldrick, *Acta Crystallogr., Sect. A: Found. Crystallogr.*, 2008, **64**, 112–122.
68 M. J. Frisch, G. W. Trucks, H. B. Schlegel, G. E. Scuseria, M. A. Robb, J. R. Cheeseman, G. Scalmani, V. Barone, G. A. Petersson, H. Nakatsuji, X. Li, M. Caricato, A. V. Marenich, J. Bloino, B. G. Janesko, R. Gomperts, B. Mennucci, H. P. Hratchian, J. V. Ortiz, A. F. Izmaylov, J. L. Sonnenberg, D. Williams-Young, F. Ding, F. Lipparini, F. Egidi, J. Goings, B. Peng, A. Petrone, T. Henderson, D. Ranasinghe, V. G. Zakrzewski, J. Gao, N. Rega, G. Zheng, W. Liang, M. Hada, M. Ehara, K. Toyota, R. Fukuda, J. Hasegawa, M. Ishida, T. Nakajima, Y. Honda, O. Kitao, H. Nakai, T. Vreven, K. Throssell, J. A. Montgomery Jr, J. E. Peralta, F. Ogliaro, M. J. Bearpark, J. J. Heyd, E. N. Brothers, K. N. Kudin, V. N. Staroverov, T. A. Keith, R. Kobayashi, J. Normand, K. Raghavachari, A. P. Rendell, J. C. Burant, S. S. Iyengar, J. Tomasi, M. Cossi, J. M. Millam, M. Klene, C. Adamo, R. Cammi, J. W. Ochterski, R. L. Martin, K. Morokuma, O. Farkas, J. B. Foresman and D. J. Fox, *Gaussian 16, Revision A.03*, Gaussian, Inc., Wallingford CT, 2016.
69 C. Lee, W. Yang and R. G. Parr, *Phys. Rev. B: Condens. Matter Mater. Phys.*, 1988, **37**, 785–789.
70 A. D. Becke, *J. Chem. Phys.*, 1993, **98**, 5648–5652.
71 P. J. Hay and W. R. Wadt, *J. Chem. Phys.*, 1985, **82**, 270–283.
72 W. R. Wadt and P. J. Hay, *J. Chem. Phys.*, 1985, **82**, 284–298.
73 P. J. Hay and W. R. Wadt, *J. Chem. Phys.*, 1985, **82**, 299–310.
74 G. A. Petersson and M. A. Al-Laham, *J. Chem. Phys.*, 1991, **94**, 6081–6090.
75 G. Scalmani and M. J. Frisch, *J. Chem. Phys.*, 2010, **132**, 114110.
76 R. Dennington, T. Keith and J. Millam, *Gauss View, Version 5*, Semichem Inc., Shawnee Mission, KS, 2009.
77 Y. Sun and S. Wang, *Inorg. Chem.*, 2009, **48**, 3755–3767.
78 Y. Sun and S. Wang, *Inorg. Chem.*, 2010, **49**, 4394–4404.
79 K. O. Christe and W. W. Wilson, *J. Fluorine Chem.*, 1990, **47**, 117–120.